Construction and Building Materials 49 (2013) 939–948

Contents lists available at SciVerse ScienceDirect

Construction and Building Materials

journal homepage: www.elsevier.com/locate/conbuildmat

Moment redistribution in continuous FRP reinforced concrete beams

Ilker Fatih Kara [a,*], Ashraf F. Ashour [b]

[a] Civil Engineering Department, Nigde University, Nigde, Turkey
[b] School of Engineering, Design and Technology, University of Bradford, Bradford BD7 1DP, UK

HIGHLIGHTS

- Under reinforced FRP sections exhibited large curvature at FRP rupture but failure was sudden.
- Over reinforced steel and FRP sections exhibited similar brittle failure but FRP sections had higher curvature at failure.
- Hogging moment redistribution over middle support is always larger than that at mid-span by around 66%.
- Continuous FRP beams demonstrated moment redistribution at concrete cracking and de-bonding between FRP and concrete.
- No moment redistribution occurred when either mid-span or middle support section reached their respective moment capacity.

ARTICLE INFO

Article history:
Available online 4 May 2013

Keywords:
Concrete beams
Continuous beams
Moment redistribution
Fibre reinforced polymer

ABSTRACT

The main purpose of this paper is to assess moment redistribution in continuous concrete beams reinforced with fibre reinforced polymer (FRP) bars. A numerical technique based on equilibrium of forces and full compatibility of strains has been developed to evaluate the moment–curvature relationships and moment capacities of FRP and steel reinforced concrete sections. Moment redistribution has then been assessed by comparing elastic and experimental moments at failure, and moment capacity at critical sections of continuous FRP reinforced concrete beams reported on the literature.

The curvature of under reinforced FRP sections was large at FRP rupture but failure was sudden, that would not allow any moment redistribution. On the other hand, FRP over reinforced sections experienced higher curvature at failure than steel over reinforced sections owing to the lower FRP modulus of elasticity. Although the experimental and elastic bending moment distributions at failure are significantly different for many beams tested elsewhere, in particular CFRP reinforced concrete beams, the experimental bending moment over the middle support at failure was far lower than the corresponding moment capacity owing to the de-bonding of FRP bars from concrete in the middle support region. Furthermore, the hogging moment redistribution over the middle support is always larger than that at mid-span by around 66%. It was also shown that the load capacity prediction of continuous FRP reinforced concrete beams using the de-bonding moment at the middle support section was the closest to the experimental failure load.

1. Introduction

Corrosion of steel reinforcement in concrete structures gives rise to cracking and spalling of concrete, resulting in costly maintenance and repair. The use of fibre reinforced polymer (FRP) as an alternative reinforcement in concrete structures has emerged as an innovative solution to such problems. In addition to their non-corrosive properties, FRPs have high strength-to-weight ratios and non-magnetic properties, making them attractive as reinforcement for concrete structures in severe environments and situations where magnetic transparency is required.

Moment redistribution in continuous members allows more flexibility in structural design. It is usually carried out by reducing the hogging moments over supports, with corresponding changes in the sagging moments to satisfy equilibrium. Accordingly, reinforcement congestion at beam to column joints in hogging zone regions may be avoided. Alternatively, when moment redistribution is employed in different load combinations, both hogging and sagging moments may be reduced, achieving economic design.

The ability of members to redistribute moments, when a critical section reaches its moment of resistance, is mainly attributed to the assumption that members possess sufficient ductility for plastic deformation to occur. As FRP reinforcing bars exhibit a linear elastic stress–strain relationship up to failure without any yielding, new ways based on deformation and energy [1,2] were proposed in the literature to evaluate the ductility index of FRP reinforced con-

* Corresponding author.
E-mail address: ifkara@nigde.edu.tr (I.F. Kara).

0950-0618/$ - see front matter © 2013 Elsevier Ltd. All rights reserved.
http://dx.doi.org/10.1016/j.conbuildmat.2013.03.094

crete members. On the other hand, few suggestions were recently introduced to improve the ductility of FRP reinforced concrete members. Wu [3] proposed the concept of compression yielding using ductile material or mechanism at the compression zone of a plastic hinge in FRP reinforced concrete members. In another investigation [4], it was shown that the presence of sufficient stirrups increased the concrete confinement in critical zones and, consequently, enhanced the concrete compression ductility. Wang and Belarbi [5] and Issa et al. [6] observed that the addition of randomly distributed polypropylene fibres to the concrete mix has improved the ductility of FRP reinforced concrete beams. A hybrid system consisting of both FRP and steel reinforcement was also introduced to improve reinforced concrete element ductility [7].

In the last two decades, several studies [8–14] investigated the flexural behaviour of simply supported FRP reinforced concrete beams. However very few, though important studies, investigated the behaviour of continuous concrete beams reinforced with FRP bars [4,15,16–19]. Based on testing of continuously supported T-section concrete beams reinforced with FRP and steel reinforcement, Grace et al. [16] concluded that beams with different FRP reinforcement arrangements demonstrated the same load capacity as steel reinforced concrete beams but the ductility and failure modes were different. Ashour and Habeeb [17,18] presented test results of continuous FRP reinforced concrete beams with different combinations of reinforcement ratios at mid-span and over middle support. The research concluded that continuously supported FRP reinforced concrete beams did not demonstrate any remarkable moment redistribution and bottom reinforcement is a key factor in controlling the behaviour of beams tested. On the other hand, Mostafa et al. [15,19] observed that moment redistribution in continuous FRP reinforced concrete beams is possible if the reinforcement configuration is properly selected.

In the present study, moment–curvature relationships and moment capacities of steel and FRP reinforced concrete sections have been predicted using a numerical technique able to capture various feature of material modelling. Moment redistribution and load capacity of continuous FRP reinforced concrete beams reported in the literature have been evaluated by considering different possibilities based on the beam ductility level.

2. Moment–curvature relationship of reinforced concrete sections

In the present study, moment–curvature relationships of FRP and steel reinforced concrete beams have been obtained by the numerical technique developed by Kara and Ashour [20] as summarized below. The moment–curvature relationships predicted are compared with these from experimental results for FRP and steel reinforced concrete beams. The main features of moment–curvature relationships are also identified for under and over steel and FRP reinforced concrete beams.

2.1. Analysis of reinforced concrete sections under bending

The cross-section of reinforced concrete members is divided into a number of concrete segments. For a particular curvature value, strains in each segment and reinforcing bars are calculated and stresses in each material are, hence, obtained from the respective stress–strain relationships. Equilibrium of forces and moments are eventually considered as explained below.

The stress–strain relationships of concrete, steel and FRP reinforcements implemented in this investigation are shown in Fig. 1. However, the numerical technique proposed can accommodate other material models. The CEB-FIP [21] model is adopted for concrete stress–strain relationship in compression as shown in Fig. 1a. This model can be represented by the following equations:

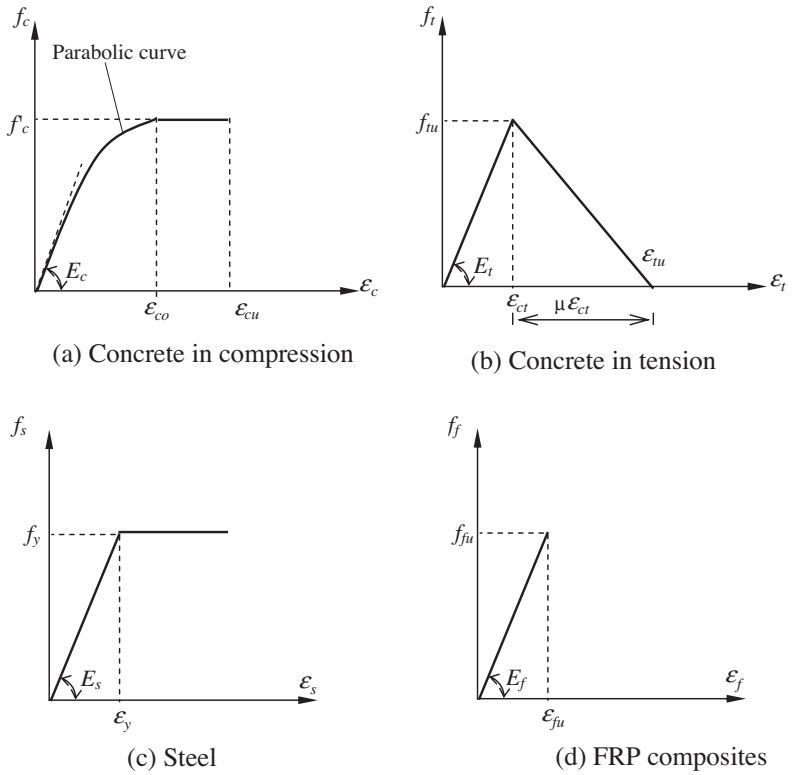

Fig. 1. FRP, steel and concrete stress–strain relationships.

$$f_c = f'_c\left(\frac{2\varepsilon_c}{\varepsilon_{co}} - \left(\frac{\varepsilon_c}{\varepsilon_{co}}\right)^2\right) \quad \varepsilon_c \leqslant \varepsilon_{co} \tag{1a}$$

$$f_c = f'_c \quad \varepsilon_{co} \leqslant \varepsilon_c \leqslant \varepsilon_{cu} \tag{1b}$$

where f_c and ε_c are the compressive stress and strain in concrete, respectively, f'_c is the cylinder compressive strength of concrete, ε_{co} (=0.002) is the strain in concrete at maximum stress and ε_{cu} (=0.0035) is the ultimate strain of concrete as shown in Fig. 1a.

A bi-linear stress–strain relationship is adopted to model concrete in tension as shown in Fig. 1b and given below:

$$f_t = E_t\varepsilon_t \quad \varepsilon_t \leqslant \varepsilon_{ct} \tag{2a}$$

$$f_t = f_{tu} - \frac{f_{tu}}{\mu\varepsilon_{ct}}(\varepsilon_t - \varepsilon_{ct}) \quad \varepsilon_{ct}(1+\mu) \geqslant \varepsilon_t > \varepsilon_{ct} \tag{2b}$$

where f_t and ε_t are the tensile stress and strain in concrete, respectively, $f_{tu}(=0.62\sqrt{f'_c})$ and ε_{ct} are the tensile strength and corresponding tensile strain of concrete, respectively, E_t is the tensile modulus of concrete, assumed to be the same as the initial tangent modulus $E_c(=2f'_c/\varepsilon_{co})$ of concrete in compression and $(\mu = (\varepsilon_{tu} - \varepsilon_{ct})/\varepsilon_{ct})$ is a factor controlling the rate of tensile strength decay, ε_{tu} is the ultimate tensile strain taken as $= 5\varepsilon_{ct}$. The tension stiffening effect is represented in the above model to account for concrete between cracks as it has a significant effect on member stiffness.

Reinforcing steel is modelled as an elastic–plastic material with yield stress f_y as shown in Fig. 1c. The stress–strain relationship of FRP bars is linear elastic up to rupture and given by:

$$f_f = E_f\varepsilon_f \quad \varepsilon_f \leqslant \varepsilon_{fu} \tag{3}$$

where f_f and ε_f are the stress and strain in FRP bars, respectively, E_f is the modulus of elasticity of FRP bars, and f_{fu} and ε_{fu} are the ultimate strength and strain of FRP bars, respectively, as shown in Fig. 1d.

Fig. 2 presents a concrete section reinforced with tensile and compressive reinforcing bars (FRP or steel), that is divided into a number of segments, n. The numerical analysis starts by assuming a small value of strain at the concrete extreme compression fibre (or tensile reinforcement). For each strain ε_c at the top level of concrete section (or strain ε_f in the tensile reinforcement), the neutral axis depth, x, is initially assumed and the correct value is iteratively obtained when equilibrium of forces is satisfied. According to the assumption that plane sections before bending remain plane and normal to the mid-surface after bending, the strain in each concrete segment is linearly proportional to its distance from the neutral axis (Fig. 2b) as expressed below:

$$\varepsilon_i = \frac{x - x_i}{x}\varepsilon_c \tag{4}$$

where ε_c is the strain at the top compression level of the reinforced concrete section and ε_i is the concrete compressive or tensile strain at mid-depth of i-th segment.

Assuming perfect bond between concrete and reinforcing bars, strains in tensile and compressive reinforcing bars can also be obtained from:

$$\varepsilon'_f = \frac{x - d'}{x}\varepsilon_c \tag{5}$$

$$\varepsilon_f = \frac{x - d}{x}\varepsilon_c \tag{6}$$

where ε_f and ε'_f indicate the strains in tensile and compressive reinforcing bars, respectively, and d and d' are the tensile and compressive reinforcement depths, respectively.

The corresponding stresses in each concrete segment, and tensile and compressive reinforcements can be calculated from the respective stress–strain relationships of concrete and reinforcing bars presented in Fig. 1. The total concrete force including the contribution of compressive and tensile forces is calculated using Eq. (7) below:

$$F_c = \sum_{i=1}^{n} f_{ci}h_i b \tag{7}$$

where f_{ci} is the concrete compressive or tensile stress at the centroid of the i-th segment, h_i (=h/n) is the thickness of the i-th segment and b is the beam width. This summation extends over all compressive and tensile segments of concrete section. The forces in tensile and compressive reinforcing bars are estimated from:

$$T_f = A_f E_f \varepsilon_f \tag{8}$$

$$C_f = A'_f E'_f \varepsilon'_f \tag{9}$$

where T_f, A_f and E_f are the force, area, and modulus of elasticity of tensile reinforcing bars, respectively, whereas C_f, A'_f and E'_f are the corresponding values of compressive reinforcement. Eqs. (8) and (9) are valid for different types of FRP bars, i.e., GFRP, AFRP and CFRP, provided that the appropriate modulus of elasticity, E_f, and tensile rupture, f_{fu}, are used. The current analysis is also developed for compressive and tensile steel reinforcement. In such case, the modulus of elasticity or the yield strength of compressive and tensile steel reinforcements is used in calculating the forces C_f and T_f, respectively. Considering equilibrium of forces, the following equation is obtained:

$$F_c + C_f = T_f$$

$$\sum_{i=1}^{n} f_{ci}h_i b + A'_f E'_f \varepsilon'_f = A_f E_f \varepsilon_f \tag{10}$$

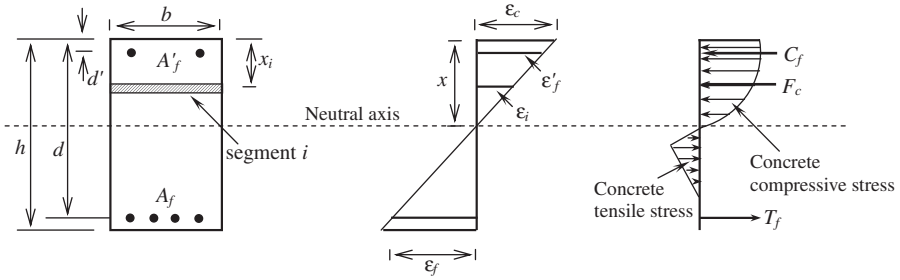

(a) FRP reinforced concrete section (b) Strain distribution (c) Stress distribution and forces

Fig. 2. Strains, stresses and forces of a reinforced concrete section.

In the above Eq. (10), the neutral axis depth x is the only unknown. The value of x is iteratively adjusted using the bi-section method and the procedure is repeated until sufficient equilibrium accuracy is attained, for example:

$$\frac{|F_c + C_f - T_f|}{|F_c|} \leqslant 10^{-8} \tag{11}$$

The curvature φ of the member can also be determined from the strain distribution as follows (see Fig. 2b):

$$\varphi = \frac{\varepsilon_c}{x} \tag{12}$$

The applied moment M_f of the section is then calculated by taking moments of internal forces about any horizontal axis, for instance about the neutral axis

$$M_f = \sum_{i=1}^{n} F_{ci}(x - x_i) + T_f(x - d) + C_f(x - d') \tag{13}$$

where F_{ci} ($=f_{ci}h_ib$) is the concrete compressive or tensile force at the centroid of the i-th segment.

The strain in the extreme concrete compression fibre (or in the tensile reinforcement) is incrementally increased and the above procedure is iteratively repeated for each strain value. The analysis is terminated when either the strain in the tensile FRP reinforcement reaches the tensile rupture strain of FRP bars ($\varepsilon_f = \varepsilon_{fu}$) or the concrete strain ε_c in the extreme compression fibre equals to the ultimate compressive strain ε_{cu} of concrete (concrete crushing). In the case of steel reinforcement, section failure is characterised by crushing of concrete (ε_c in the extreme concrete compression fibre = ε_{cu}) before or after yielding of tensile steel reinforcement. The section moment capacity M_{fu} is, therefore, the highest moment attained by the section for various increments considered until failure. Based on the aforementioned procedure, a computer program has been developed for the moment–curvature relationships and moment capacities of FRP and steel reinforced concrete sections.

2.2. Validation of the predicted moment–curvature relationship against experiments

The moment–curvature relationships predicted from the above technique are compared with the experimental results of the steel and FRP reinforced concrete simply supported beams tested by Thiagarajan [22] and Srikanth et al. [23] as presented in Fig. 3a for steel and Fig. 3b for FRP reinforcement. Geometrical dimensions, reinforcement details and material properties of the beams considered in Fig. 3 are given in Table 1. The numerical results obtained from the present technique compare well with the test results for both steel and FRP reinforced concrete beams as depicted in Fig. 3. The numerical technique is also able to accurately predict various features of the moment–curvature relationships including the first cracking load, yielding of steel, post yielding, rupture of FRP bars and concrete crushing. In addition, the moment capacities of both steel and FRP reinforced concrete beams are reasonably predicted by the proposed technique.

The validity of the above technique is further examined by considering the effect of tensile strength and tension stiffening of concrete on the moment curvature relationships of beams B4 and B9 (Fig. 4a and b) and also the effect of the number of section segments on their moment capacities (Fig. 4c). Fig. 4a and b indicates that the tensile strength has a large effect on the initial stiffness before the first crack occurrence but, at higher moments, the predictions are almost identical for all the cases considered (with and without tensile strength and/or tension stiffening). Fig. 4c also shows that the number of the beam section segments between

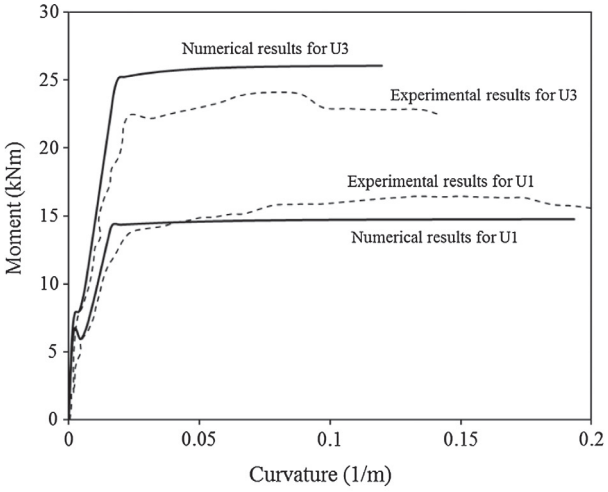

(a) Steel reinforced concrete beams

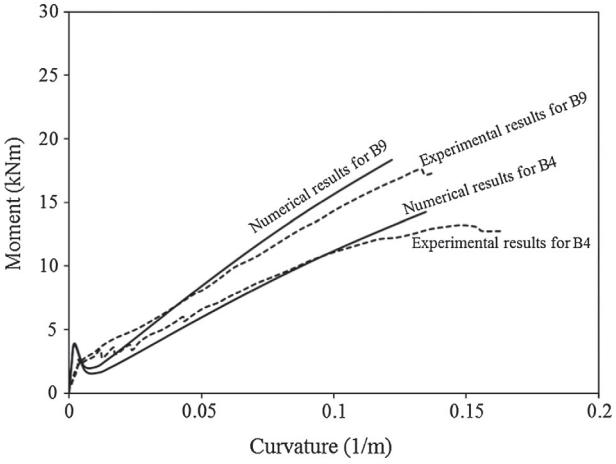

(b) FRP reinforced concrete beams

Fig. 3. Comparison of predicted and experimental moment–curvature relationships of simply supported reinforced concrete beams.

10 and 100 has a negligible effect on the moment capacities of beams B4 and B9.

2.3. Effect of reinforcement type on moment–curvature relationship

The present numerical technique has been employed to study the effect of type of reinforcement (FRP or steel) on the moment–curvature relationship of concrete beams as predicted in Fig. 5: Fig. 5a for under reinforced and Fig. 5b for over reinforced sections. The dimensions and concrete properties are the same for all sections considered in Fig. 5; b = 200 mm, h = 300 mm and f_c' = 30 N/mm^2. The amount of steel and FRP reinforcement in each case was selected to achieve the same tensile capacity; i.e. $A_f f_{fu}$ for GFRP or CFRP = $A_s f_y$ for steel (=173 kN for under-reinforced or 777 kN for over-reinforced section); where A_f and A_s are the area of tensile FRP and steel reinforcement, respectively; f_{fu} is the ultimate strength of FRP and f_y is the yield strength of steel. Fig. 5a shows that all the three beams have a similar behaviour at early stages of loading. However, the first cracking loads were slightly different owing to the variation in the modulus of elasticity of reinforcing bars. After the first crack had occurred, some stress redistribution took place as more loads were suddenly transferred from

Table 1
Details of the simply and continuously supported reinforced concrete beams reported in the literature.

Reference	Beam notation	Supporting condition	Loading type	b (mm)	h (mm)	l (mm)	Reinforcing bars (mm)		E_f (kN/mm^2)	f'_c (N/mm^2)
							Top	Bottom		
[22]	B4	SS	Two point	152.4	152.4	1524	2Φ12.7 (Steel)	2Φ6.35 (CFRP)	140	51.7
[22]	B9	SS	Two point	152.4	152.4	1524	2Φ12.7 (Steel)	2Φ7.94 (CFRP)	140	53.3
[23]	U1	SS	Two point	150	200	1800	2Φ4 (Steel)	2Φ12 (Steel)	200 (Steel)	42.5
[23]	U3	SS	Two point	150	200	1800	2Φ4 (Steel)	2Φ16 (Steel)	200 (Steel)	47.9
[18]	GcUO	CS	Mid-span	200	300	2750	3Φ12.7 (GFRP)	6Φ15.9 (GFRP)	38.7 (for Φ15.9) 44.2 (for Φ12.7)	29.0
[18]	GcOO	CS	Mid-span	200	300	2750	6Φ15.9 (GFRP)	6Φ15.9 (GFRP)	38.7	25.0
[18]	GcOU	CS	Mid-span	200	300	2750	6Φ15.9 (GFRP)	3Φ12.7 (GFRP)	38.7 (for Φ15.9) 44.2 (for Φ12.7)	29.0
[17]	C-C-3	CS	Mid-span	200	300	2750	2Φ12 (CFRP)	2Φ7.5 (CFRP)	200	23.6
[17]	C-C-4	CS	Mid-span	200	300	2750	2Φ7.5 (CFRP)	2Φ12 (CFRP)	200	27.2
[17]	C-C-5	CS	Mid-span	200	300	2750	2Φ12 (CFRP)	2Φ12 (CFRP)	200	28.0
[15]	GS1	CS	Mid-span	200	300	2800	2Φ16 (GFRP)	3Φ16 (GFRP)	46.0	28.0
[15]	GS2	CS	Mid-span	200	300	2800	3Φ16 (GFRP)	2Φ16 (GFRP)	46.0	26.0
[19]	GSu-8d/3p	CS	Mid-span	200	300	2800	2Φ16 (GFRP)	3Φ16 (GFRP)	46.0	32.0
[19]	GSu-10d/2p	CS	Mid-span	200	300	2800	2Φ16 (GFRP)	3Φ16 (GFRP)	46.0	33.0
[19]	GGu-10d/2p	CS	Mid-span	200	300	2800	2Φ16 (GFRP)	3Φ16 (GFRP)	46.0	27.0
[19]	GGu-10d/3p	CS	Mid-span	200	300	2800	2Φ16 (GFRP)	3Φ16 (GFRP)	46.0	32.0
[19]	GSs-10d/2p	CS	Mid-span	200	300	2800	4Φ16 (GFRP)	7Φ16 (GFRP)	46.0	33.0
[15]	CS1	CS	Mid-span	200	300	2800	4Φ10 (CFRP)	3Φ10 (CFRP)	116	27.0
[19]	CSu-8d/2e	CS	Mid-span	200	300	2800	2Φ10 (CFRP)	3Φ10 (CFRP)	116	26.0

Note: b, h and l = width, depth and span of beams, respectively, E_f is the modulus of elasticity of longitudinal reinforcement and f'_c is the cylinder compressive strength. SS and CS indicate simply and continuously supported beams, respectively.

cracked concrete to the reinforcing bars and consequently, the influence of the modulus of elasticity of reinforcing bars became more apparent as each reinforced concrete section showed significantly different flexural stiffness. However, all sections exhibited the same moment of resistance as all reinforcements have the same axial tensile capacity. Fig. 5a also indicates that, although the steel reinforced concrete section yielded at a relatively small curvature, the ductility of steel reinforcement allowed significant curvature increase at the same moment capacity and consequently, larger rotational capacity at failure. On the other hand, the curvature at FRP rupture was large but sudden (see Fig. 5a), that would not allow any moment to be redistributed to other sections along the beam. For over reinforced sections, all sections exhibited brittle failure mode and different moment capacities as failure is controlled by concrete crushing and elastic modulus of reinforcing bars. However, FRP reinforced concrete sections experienced higher curvature at failure owing to their lower modulus of elasticity. After the first crack, the flexural stiffness is highest for steel, then CFRP, followed by GFRP, depending on their respective modulus of elasticity.

3. Moment redistribution in continuous reinforced concrete beams

Generally, steel under-reinforced continuous beams have the ability to redistribute bending moment at failure between critical sections due to yielding of steel reinforcement as depicted in Fig. 5a. However, the brittle nature of FRP reinforcements raises concerns about their ability to redistribute moments in continuous members.

In this section, the moment redistribution in FRP reinforced concrete continuous beams available in the literature [4,15–19] is investigated. Geometrical dimensions, reinforcement details and material properties of FRP reinforced concrete continuous beams considered are given in Table 1. Each continuous beam consisted of two equal spans, was loaded by a single point load at the middle of each span and was reinforced with different combinations of either GFRP or CFRP bars at the top and bottom layers. The reinforcement arrangement has affected the mode, load and location of beam failure as reported in different experimental investigations [4,15–19].

For the two span beams reported in the literature, the elastic bending moments at the critical sections are $0.156Pl$ at mid-span and $0.188Pl$ over the middle support, where P and l are the mid-span applied load and beam span, respectively, as shown in Fig. 6. It is to be noted that the above bending moment values are calculated based on a uniform flexural stiffness along the beam span. However, occurrence of concrete cracks at different load levels reduces the beam flexural stiffness at different locations and, consequently, the bending moment distribution changes too. When the magnitude of the applied load is increased enough for the moment at either mid-span or middle support section to reach the section moment capacity, there are three different possibilities based on the beam ductility level as explained below:

- For a fully ductile beam, a plastic hinge develops at a critical section to activate the plastic moment of resistance. As the load P is further increased, the moments at other critical sections also increase until eventually reach the plastic moments of resistance, causing the beam to collapse. The flexural load capacity in such case is based on a collapse mechanism with plastic hinges at mid-span and central support sections. Thus, the fiexural load capacity P_u on each span would be calculated from:

$$P_u = \frac{2}{l}(M_{uh} + 2M_{us}) \tag{14}$$

Where M_{us} and M_{uh} are the moment capacities at mid-span and middle support sections, respectively.

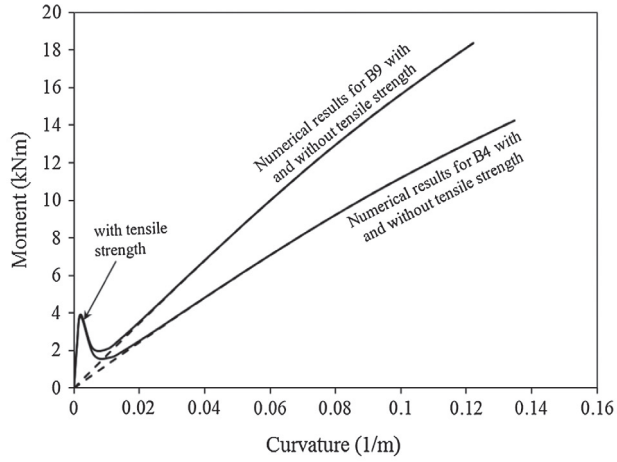

(a) Effect of tensile strength

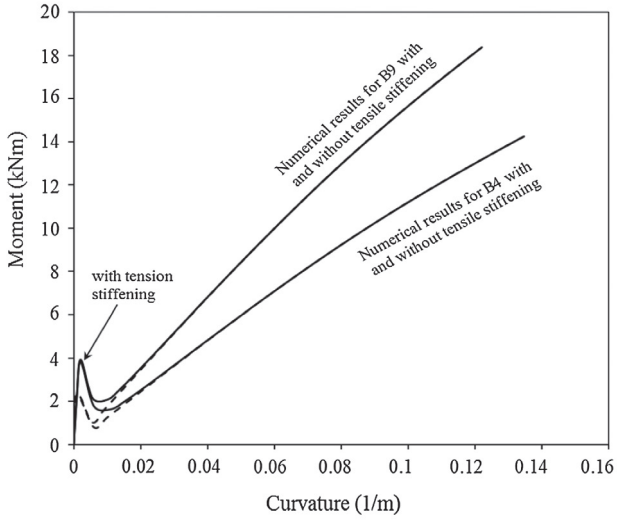

(b) Effect of tension steffening

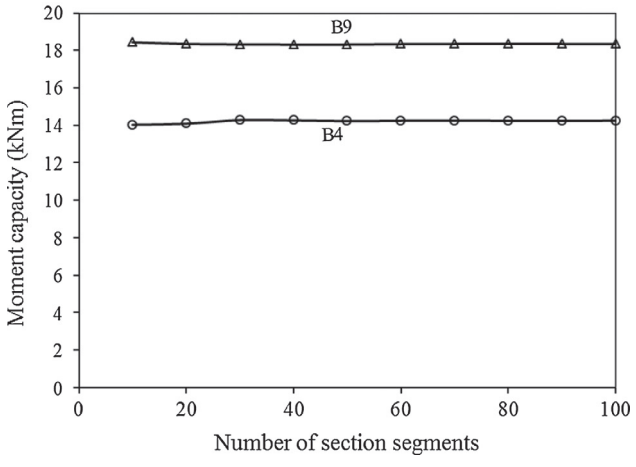

(c) Effect of cross sectional segments

Fig. 4. Effect of concrete modelling in tension and section segments number on the technique prediction.

- For a brittle elastic material, the beam is suddenly failed when either the mid-span or middle support section reaches the moment of resistance. Thus, the flexural load capacity P_u on each span is the smaller of $M_{us}/0.156l$ and $M_{uh}/0.188l$ and no moment redistribution is possible.

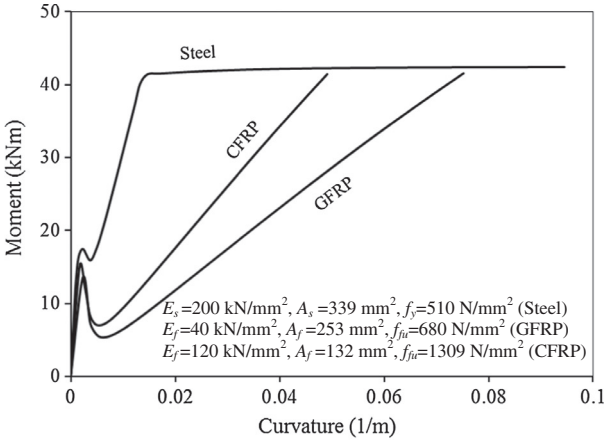

(a) Under reinforced beam sections

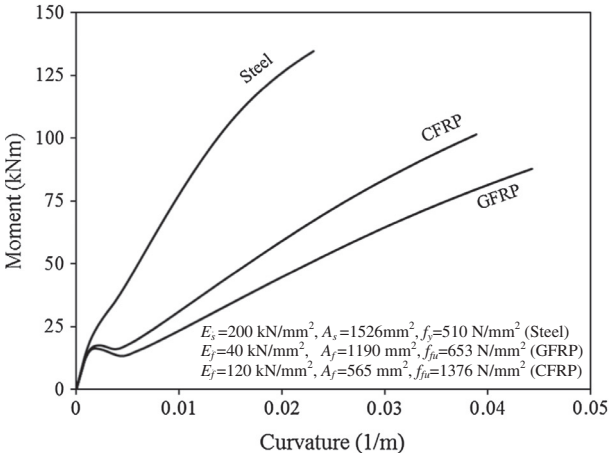

(b) Over reinforced beam sections

Fig. 5. Moment–curvature relationships of under and over FRP and steel reinforced concrete sections.

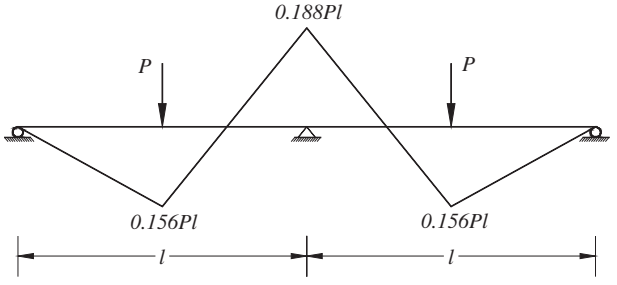

Fig. 6. Elastic bending moment distribution assuming constant flexural stiffness.

- For a semi-ductile beam, a limited moment redistribution occurs depending on the moment–curvature relationship of materials. The flexural load capacity P_u on each span can be calculated from Eq. (14) above with either M_{us} or M_{uh} replaced with the corresponding moment of resistance and the other with the limited moment of resistance at failure. For example, where de-bonding between FRP reinforcement and concrete occurred as reported in CFRP reinforced concrete continuous beam tests [15,17,19], a limited moment of resistance over the middle support, at which de-bonding occurs, should be used in Eq. (14).

Table 2
Experimental bending moment at failure, predicted moment capacity and moment redistribution factor at failure of the continuous FRP reinforced concrete beams reported in the literature.

Beam notation	Experimental moment at failure (kN m)		Predicted moment capacity (kN m)		Experimental/predicted moment ratio		Moment redistribution (MR%) (Eq. (15))		λ = MR (hogging)/ MR (sagging)
	Midspan	Middle support	Midspan	Middle support	Midspan	Middle support	Mid-span	Middle support	
GcOU	60.5	78.5	56.3	88.2	1.08	0.89	3.51	−5.78	−1.65
GcOO	86.9	55.1	86.2	86.2	1.01	0.64	−20.7	35.3	−1.70
GcUO	97.6	30.8	88.2	56.3	1.10	0.55	−37.5	63.3	−1.69
GS1	60.2	49.0	64.9	54.8	0.93	0.89	−14.0	23.0	−1.64
GS2	46.3	63.4	52.6	62.3	0.88	1.02	4.90	−8.00	−1.63
GSu-8d/3p	74.9	46.9	70.1	58.9	1.07	0.80	−22.4	36.4	−1.62
GSu-10d/2p	72.0	50.0	71.6	59.9	1.01	0.84	−18.0	31.7	−1.76
GGu-10d/2p	57.3	41.2	63.6	53.7	0.91	0.77	−18.1	29.0	−1.60
GGu-10d/3p	66.0	47.2	70.1	58.8	0.94	0.80	−17.9	30.0	−1.68
GSs-10d/2p	105	70.8	88.8	77.4	1.19	0.91	−19.3	33.0	−1.71
CS1	51.8	29.0	60.7	45.2	0.85	0.64	−25.1	41.8	−1.67
CSu-8d/2e	51.8	60.2	63.4	70.6	0.81	0.85	−1.37	2.27	−1.66
CC3	44.8	14.0	42.5	56.2	1.05	0.25	−37.9	63.7	−1.68
CC4	60.7	7.89	56.7	42.8	1.07	0.18	−49.5	83.5	−1.69
CC5	56.0	12.1	56.9	56.9	0.99	0.21	−43.7	73.8	−1.69

Moment redistribution is assessed by comparing elastic and experimental moments at failure, and moment capacity at critical sections of FRP reinforced concrete continuous beams reported in the literature. The moment redistribution factor, *MR*, from one critical section to another can be obtained from:

$$MR\% = \frac{M_e - M_u}{M_e} \times 100 \tag{15}$$

where M_e and M_u are the critical section elastic and ultimate moments at failure.

The predicted moments of resistance, experimental moment at failure and moment redistribution factor obtained from Eq. (15) at failure for both mid-span and middle support critical sections are presented in Table 2. The predicted moment of resistance and experimental moment at failure as well as the elastic moment calculated for the experimental failure load are also plotted in Fig. 7a for GFRP reinforced concrete beams and Fig. 7b for CFRP reinforced concrete beams. The experimental and elastic bending moments at both middle support and mid-span sections were calculated from the support reaction and mid-span applied load measured at failure in each test.

Table 2 indicates that the moment redistribution factor, *MR*, at middle support sections is always larger than that of mid-span sections. This observation is investigated further below. Although Eq. (14) is expressed at the beam failure, this is a generic equilibrium condition that is valid at any applied load between zero and failure. It can also be re-stated in terms of increments of load and moment as follows:

$$\frac{l}{2}\Delta P = \Delta M_h + 2\Delta M_s \tag{16}$$

where ΔM_h and ΔM_s are moment increments at mid-span and middle support sections due to a mid-span point load increment ΔP. Considering moment redistribution at a given section under a given magnitude of load, then the load increment $\Delta P = 0$ and therefore, the relation between ΔM_h and ΔM_s can be written in the following form:

$$\Delta M_h = -2\Delta M_s \tag{17}$$

The hogging and sagging moment redistributions can be written as ($\Delta M_h/0.188Pl$) and ($\Delta M_h/0.156Pl$), respectively. Considering Eq. (17), thus, the ratio λ of hogging to sagging moment redistributions can be evaluated as:

$$\lambda = \frac{\Delta M_h}{0.188Pl} \Big/ \frac{\Delta M_s}{0.156Pl} = \frac{0.156\Delta M_h}{0.188\Delta M_s} = \frac{0.156(-2\Delta M_s)}{0.188\Delta M_s} = -2 \times 0.156/0.188 = -1.66 \tag{18}$$

Eq. (18) indicates that the hogging moment redistribution should always be 66% more than the negative of the sagging moment redistribution provided that the ratio between hogging and sagging bending moments is the same as that obtained from elastic analysis assuming constant flexural stiffness throughout the beam length. The results of λ presented in Table 2 for beams considered do indeed very nearly satisfy this relationship, except for the results of GSu-10d/2p (76% more) and GGu-10d/2p (60% more). This may be attributed to the ratio between the hogging and sagging bending moments at failure for these two beams.

In most cases, the mid-span sections have reached or were close to achieving their predicted moment of resistance as indicated in Table 2; the ratio between the experimental moment at failure, M_{exp}, and predicted moment of resistance, M_{pred}, ranged from 0.81 to 1.19. On the other hand, the majority of middle support sections in CFRP reinforced concrete beams were far from achieving their moment of resistance (M_{exp}/M_{pred} range = 0.18–0.85) due to the apparent de-bonding of CFRP bars and concrete as reported in the experimental testing [15,17–19]. However, middle support sections in GFRP reinforced concrete beams achieved a relatively closer moment at failure to their predicted moment of resistance (M_{exp}/M_{pred} range = 0.55–1.02). Fig. 7 indicates that the experimental bending moment distribution at failure is significantly different from that obtained from linear elastic analysis for the failure load for many beams, especially CFRP beams as depicted in Fig. 7b. Furthermore, redistribution of moment from the middle support section to the mid-span section occurred for all CFRP reinforced concrete beams. However, redistribution of moment from the mid-span section took place in only two GFRP reinforced concrete beams, namely GcOU and GS2. In all cases considered, no middle support section reached its predicted moment of resistance as also given in Table 2. This is mainly attributed to the early wide cracks developed at the middle support section of these beams owing to the slippage between top reinforcement and surrounding concrete as reported in the experimental investigations [15,17,19]. The above results indicate that when the middle support section reached the de-bonding moment, the continuous beam did not fail until the mid-span section also failed.

The moment redistribution is further assessed by comparing the experimental load capacity against the calculated load capacities based on the above three assumptions as presented in Table 3. The three load capacities are calculated from Eq. (14) using the moments of resistance of mid-span and middle support sections, from Eq. (14) using the moment of resistance of the mid-span section and the de-bonding moment at failure at the middle support sec-

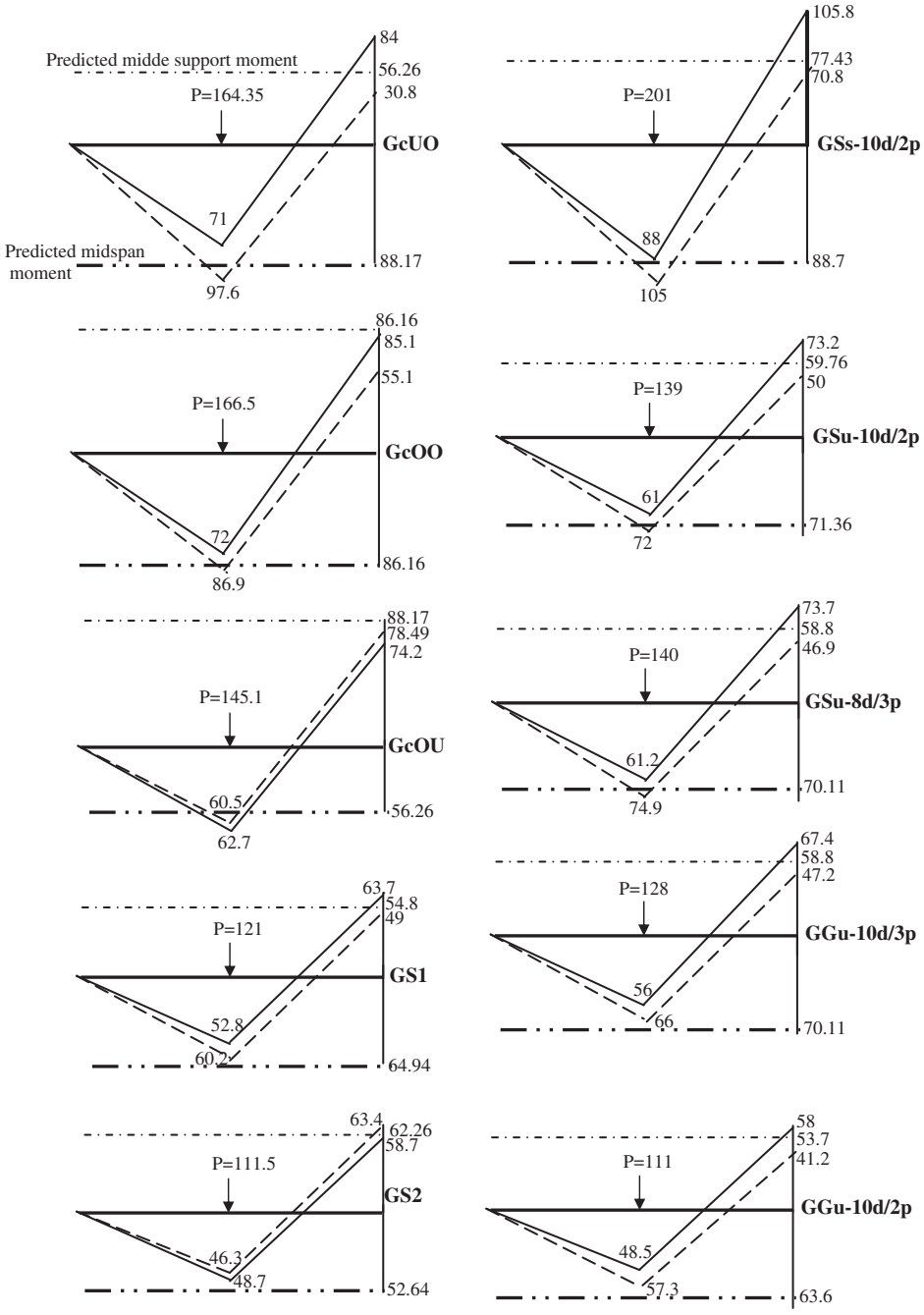

(a) GFRP beams

Fig. 7. (a and b) Experimental and elastic bending moment distributions at failure, and moments of resistance at critical sections of beams reported in the literature.

tion, and the lower load that would achieve the moment of resistance at either the mid-span or middle support section. The debonding moment at failure used in Eq. (14) is obtained from the experimental results at failure in each test. As shown in Table 3, the theoretical failure load obtained from Eq. (14) using the debonding moment at the middle support gives the closest result for both GFRP and CFRP beams to the experimental failure loads, with an average and standard deviation between the experimental and predicted load capacities of 0.996% and 7.6%, respectively. However, the load capacity calculated based on the moment capacities at mid-span and middle support sections overestimated the experimental failure load, especially for CFRP continuous beams; the average and standard deviation between the experimental and predicted load capacities for all beams are 0.894% and 10.1%, respectively. On the other hand, the load capacity calculated based on elastic brittle material slightly underestimated the experimental failure load with an average and standard deviation between the experimental and predicted load capacities of 1.086% and 20.3%, respectively. Although the experimental and elastic moments at failure are significantly different in few cases indicating major moment redistribution, the experimental failure load was lower than that predicted using the mid-span and middle support moments of resistance, for example, a significant moment redistribution from the middle support sections in beams C–C-3, C–C-4

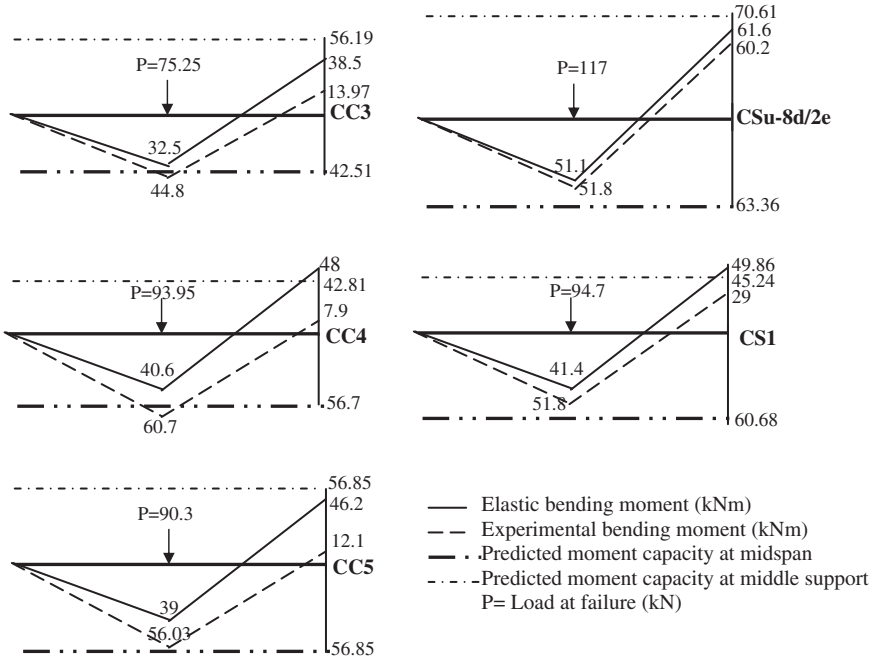

(b) CFRP beams

Fig. 7. (*continued*)

Table 3
Experimental and predicted failure loads of the continuous FRP reinforced concrete beams reported in the literature.

Beam notation	Experimental failure load, P_{exp} (kN)	Predicted failure load (kN)			Experimental/predicted failure load ratio		
		P_{fd}	P_{sd}	P_{bem}	P_{exp}/P_{fd}	P_{exp}/P_{sd}	P_{exp}/P_{bem}
GcOU	145.0	146.0	138.9	131.1	0.99	1.04	1.11
GcOO	166.5	188.0	165.4	168.7	0.89	1.00	0.99
GcUO	164.4	169.2	150.7	108.8	0.97	1.09	1.51
GS1	121.0	131.9	127.8	123.4	0.92	0.95	0.98
GS2	111.5	119.7	120.5	118.3	0.93	0.93	0.94
GSu-8d/3p	140.0	142.2	133.7	111.9	0.98	1.05	1.25
GSu-10d/2p	139.0	145.0	138.0	113.6	0.96	1.00	1.22
GGu-10d/2p	111.0	129.2	120.3	102.0	0.86	0.92	1.09
GGu-10d/3p	128.0	142.2	133.9	111.7	0.90	0.96	1.15
GSs-10d/2p	201.0	182.1	177.4	147.1	1.10	1.13	1.37
CS1	94.7	119.0	107.4	85.9	0.80	0.88	1.10
CSu-8d/2e	117.0	141.0	133.5	134.2	0.83	0.88	0.87
CC3	75.3	102.7	72.0	99.2	0.73	1.05	0.76
CC4	94.0	113.6	88.2	82.8	0.83	1.07	1.13
CC5	90.3	124.0	91.5	110.0	0.73	0.99	0.82
Average					0.894	0.996	1.086
Standard deviation					10.1%	7.6%	20.3%

P_{fd}, P_{sd} and P_{bem} are predicted failure loads based on fully ductile, semi-ductile using de-bonding moment at the middle support and brittle elastic materials, respectively.

and C–C-5 as shown in Fig. 7b but the ratios of the experimental and predicted failure loads assuming the moment of resistance at both mid-span and middle support sections for the three beams are 0.73, 0.83 and 0.73, respectively. As the de-bonding moment is not easily predicted with high accuracy, the load capacity prediction based on achieving moment capacity at either mid-span or middle support section is closer to the experimental load capacity and also safer than that from assuming moments of resistance at both mid-span and middle support sections.

4. Conclusions

Moment redistribution of FRP reinforced concrete continuous beams has been assessed by comparing elastic and experimental moments at failure, and moment capacity at critical sections of FRP reinforced concrete continuous beams reported in the literature. Moment–curvature relationships for various steel and FRP reinforced concrete sections have been developed from equilibrium of forces and full compatibility of strains. The following conclusions may be drawn:

- The curvature of under reinforced FRP sections was large at FRP rupture but failure was sudden, which would not allow any moment redistribution.
- Over reinforced steel and FRP sections exhibited similar brittle failure. However, FRP over reinforced sections experienced higher curvature at failure owing to the lower FRP modulus of elasticity than that of steel reinforcement.

- Although the experimental bending moment distribution at failure is different from that obtained by elastic analysis for many beams, especially CFRP beams, the experimental bending moment at failure over the middle support was far lower than the predicted moment of resistance.
- Hogging moment redistribution over the middle support is always larger than that at the mid-span by around 66%.
- Load capacity predictions for the two-span FRP reinforced concrete beams reported in the literature using the de-bonding moment at the middle support section was the closest to the experimental failure load. Furthermore, load capacity prediction using moment of resistance at either mid-span or middle support section is closer to the experimental load at failure, and safer than using moments of resistance at both critical sections.
- Continuous FRP reinforced concrete beams demonstrated moment redistribution when cracking and de-bonding between FRP and concrete occurred. However, no moment redistribution occurred when either the mid-span or middle support section reached their respective moment capacity owing to the brittle nature of FRP reinforcement rupture or concrete crushing.

References

[1] Vijay PV, GangaRao HV. Bending behaviour and deformability of glass fiber-reinforced polymer reinforced concrete members. ACI Struct J 2001;98(6):834–42.
[2] Theriault M, Benmokrane B. Effects of FRP reinforcement ratio and concrete strength on flexure behaviour of concrete beams. J Compos Constr 1998;2(1):7–16.
[3] Wu YF. New avenue of achieving ductility for reinforced concrete members. J Struct Eng, ASCE 2006;132(9):1502–6.
[4] Matos B, Correia JR, Castro LMS, França P. Structural response of hyperstatic concrete beams reinforced with GFRP bars: effect of increasing concrete confinement. Compos Struct 2012;94:1200–10.
[5] Wang H, Belarbi A. Ductility characteristics of fiber-reinforced-concrete beams reinforced with FRP rebars. Constr Build Mater 2011;25:2391–401.
[6] Issa MS, Metwally IM, Elzeiny SM. Influence of fibers on flexural behavior and ductility of concrete beams reinforced with GFRP rebars. Eng Struct 2011;33:1754–63.
[7] Yoon Y-S, Yang J-M, Min K-H, Shin H-O. Flexural strength and deflection characteristics of high-strength concrete beams with hybrid FRP and steel bar reinforcement. ACI special, publication, SP-275-04; 2011. p. 1–22.
[8] Almusallam TH. Analytical prediction of flexure behavior of concrete beams reinforced with FRP bars. J Compos Mater 1997;31(7):640–57.
[9] Al-Sayed SH. Flexure behaviour of concrete beams reinforced with GFRP bars. Cem Concr Compos 1998;20(1):1–11.
[10] Al-Sayed SH, AL-Salloum YA, Almusallam TH. Performance of glass fibre reinforced plastic bars as a reinforcing material for concrete structures. Composites, Part B 2000;31(6–7):555–67.
[11] Benmokrane B, Chaallal O, Masmoudi R. Glass fiber reinforced plastic (GFRP) rebars for concrete structures. Constr Build Mater 1995;9(6):353–64.
[12] Benmokrane B, Chaallal O, Masmoudi R. Flexural response of concrete beams reinforced with FRP reinforcing bars. ACI Struct J 1996;93(1):46–53.
[13] Pecce M, Manfredi G, Cosenza E. Experimental response and code models of GFRP RC beams in bending. J Compos Constr 2000;4(4):182–7.
[14] Masmoudi R, Thériault M, Benmokrane B. Flexural behavior of concrete beams reinforced with deformed fiber reinforced plastic reinforcing rods. ACI Struct J 1998;95(6):665–76.
[15] Mostafa EM, Amr ER, Ehab ES. Flexural behavior of continuous FRP reinforced concrete beams. J Compos Constr 2010;14(6):669–80.
[16] Grace NF, Soliman AK, Abdel-Sayed G, Saleh KR. Behavior and ductility of simple and continuous FRP reinforced beams. J Compos Constr 1998;2(4):186–94.
[17] Ashour AF, Habeeb MN. Continuous concrete beams reinforced with CFRP bars. Struct, Build 2008;SB6:349–57.
[18] Habeeb MN, Ashour AF. Flexural behavior of continuous GFRP reinforced concrete beams. J Compos Constr 2008;12(1):115–24.
[19] Mostafa EM. Behaviour of continuous concrete beams reinforced with FRP bars, PhD thesis. University of Manibota; 2011. p. 198.
[20] Kara IF, Ashour AF. Flexural performance of FRP reinforced concrete beams. Compos Struct 2012;94:1616–25.
[21] CEB-FIP. Model code for concrete structures, Comite Euro-International du Beton, Bulletin 213/214; 1990.
[22] Thiagarajan G. Experimental and analytical behavior of carbon fiber-based rods as flexural reinforcement. J Compos Constr 2003;7(1):64–72.
[23] Srikanth M, Kumar GR, Giri S. Moment curvature of reinforced concrete beams using various confinement models and experimental validation. Asian J Civ Eng 2007;8(3):247–65.